MRS Advances (2025) 10:2453–2460
https://doi.org/10.1557/s43580-025-01314-8

ORIGINAL PAPER

First-principles investigation of structural, mechanical, electronic, and thermal properties of half-Heusler ZrPtSn

Lynet Allan[1] · Julius M. Mwabora[1] · Winfred M. Mulwa[2] · R. E. Mapasha[3] · Robinson J. Musembi[1]

Received: 25 February 2025 / Accepted: 30 May 2025 / Published online: 30 June 2025
© The Author(s) 2025

Abstract

This study explores the structural, mechanical, electronic, lattice dynamical, and thermal properties of the half-Heusler ZrPtSn using first-principles density functional theory. The goal is to assess its suitability for electronic and thermoelectric applications. Structural optimization confirmed stability under ambient conditions. Mechanical properties, including bulk, shear, and Young's moduli, were evaluated for stiffness and ductility. Electronic structure analysis determined its semiconducting nature, with band gaps of 1.10 eV (without SOC) and 0.95 eV (with SOC). Phonon dispersion was analyzed to assess dynamical stability. ZrPtSn was dynamically stable, with no imaginary phonon modes. Its band gap suggests potential for optoelectronic applications. These findings provide a comprehensive understanding of ZrPtSn's properties, supporting its potential use in electronic and thermoelectric devices and paving the way for further experimental and theoretical studies.

Introduction

Due to increasing energy demands, thermoelectric (TE) materials have gained significant attention for their ability to convert heat into electricity and vice versa. This property is highly utilized in cooling and power generation applications. Among various TE materials, semiconductors are considered the most promising candidates [1, 2]. These elements, primarily found in groups 3 to 5 of the periodic table, include binary alloys such as GaSb and AlSb, which exhibit semiconducting properties at room temperature [3]. However, ternary compounds [4] often display superior semiconducting properties compared to binary and elementary semiconductors.

Transition metal alloys, particularly Heusler alloys, represent a crucial class of ternary materials due to their ordered and stable nature. These alloys crystallize in a cubic MgAgAs-type structure with space group number 216 [5]. Heusler alloys are divided into full-Heusler (FH) and half-Heusler (HH) compounds. FH alloys have the atomic composition X_2YZ, while HH alloys follow XYZ, where X and Y are transition metals, and Z is a semiconductor element. HH alloys have gained interest due to their applications in thermoelectric devices, spintronics, and superconductors [6, 7]. Despite their potential, HH alloys face challenges related to mechanical and dynamical instability.

Most existing studies on 18-valence electron HH compounds have focused on alloys like TiCoSb, ZrCoSb, and MNiSn, which have demonstrated promising thermoelectric performance. However, ZrPtSn remains largely unexplored despite its comparable electron count and structural configuration. The inclusion of platinum, a heavier, less commonly studied transition metal, introduces significant relativistic effects and enhanced spin–orbit coupling, which may alter its electronic and thermal transport behavior. Furthermore, Sn as the group 14 element provides a broader energy gap window compared to Sb or Sn counterparts in similar alloys. This unique combination of Zr, Pt, and Sn positions ZrPtSn as a candidate with potentially superior or complementary mechanical and electronic characteristics, warranting a detailed first-principles investigation. This study provides a comprehensive analysis of the structural, mechanical, electronic, and thermal properties of ZrPtSn to bridge existing knowledge gaps.

This study focuses on investigating the structural, electronic, mechanical, dynamical, and thermal properties of

✉ Lynet Allan
allanlynet3@students.uonbi.ac.ke

[1] Department of Physics, Faculty of Science and Technology, University of Nairobi, Chiromo, P.O. Box 30197-00100, Nairobi, Kenya

[2] Department of Physics, Faculty of Science, Egerton University, Egerton, P.O. Box 536-20115, Njoro, Kenya

[3] Department of Physics, University of Pretoria, Hatfield, Private Bag X20, Pretoria, South Africa

the HH alloy ZrPtSn using first-principles calculations. Recent research has concentrated on HH compounds with eighteen valence electrons, utilizing the semi-classical Boltzmann transport equation and density functional theory (DFT) techniques [8]. ZrCoSb, for instance, has been extensively studied experimentally and computationally [7, 9]. The optimized lattice parameter of ZrPtSn is found to be 6.46 Å without SOC and 6.47 Å with SOC, which aligns well with theoretical predictions. The calculated band gap is 1.10 eV without SOC and 0.95 eV with SOC, indicating semiconducting behavior. These findings are consistent with those of Sekimoto et al. who experimentally analyzed the powder X-ray diffraction patterns of annealed $TiCoSn_xSb_{1-x}$ ($x = 0.0$, 0.01, and 0.05) and confirmed a stable cubic phase across all samples. Only the sample with $x = 0.05$ exhibited traces of a second phase. They experimentally determined lattice parameters were 5.8818, 5.8835 and 5.8829 Å for $x = 0.0$, 0.01, and 0.05, respectively. The agreement between our computational results for ZrPtSn and Sekimoto et al.'s experimental trends [1] on related Heusler systems reinforces the structural reliability and semiconducting nature of these materials.

Recent studies on HH alloys with compositions such as MNiSn (M = Ti, Zr, Hf) suggest that Zr-based HH alloys possess a higher figure of merit ($ZT > 1$), making them superior candidates for thermoelectric applications [10, 12]. However, the stability of MNiSn and MCoSb HH alloys remains underexplored. Since thermoelectric applications often involve extreme temperature fluctuations, understanding the mechanical and dynamical stability of HH alloys is essential. Materials with higher toughness and mechanical strength are better suited to withstand vibrational stress and thermal cycling, enhancing their commercial viability.

Mechanical stability can be theoretically assessed through elastic constants, which play a critical role in verifying stability criteria and other structural parameters. Evaluating the behavior of HH materials under strain provides insights into thermal expansion, atomic bonding, and overall structural stability. This study specifically examines the elastic properties of ZrCoY (Y = Sb, Bi) to assess their potential as thermoelectric materials. The elastic constants, elastic moduli, and lattice dynamics of these HH compounds have been computed and analyzed. Phonon dispersion curves confirm the dynamical stability of these materials, while band structure calculations validate their narrow bandgap semiconductor nature, reinforcing their suitability for thermoelectric applications.

Methods

Simulations on the cubic half-Heusler alloy ZrPtSn were conducted using density functional theory (DFT) within the Quantum ESPRESSO (QE) package [2]. The Perdew-Burke-Ernzerhof (PBE) formulation of the generalized gradient approximation (GGA) [3] using the Perdew-Burke-Ernzerhof (PBE) parameterization. We employed projector augmented-wave (PAW) pseudopotentials for all elements involved (Zr, Pt, and Sn), ensuring accurate treatment of core-valence interactions. For calculations without spin–orbit coupling (SOC), scalar-relativistic PAW pseudopotentials were used. In contrast, for SOC-inclusive calculations, fully relativistic PAW pseudopotentials were adopted to incorporate spin–orbit effects accurately. Structural relaxations were carried out until the forces on each atom were less than 10^{-4} Ry/Bohr, and the total energy difference between successive steps was below 10^{-6} Ry. These parameters were tested to ensure convergence and reliability of the computed properties. Lattice constant optimization was performed by fitting data to the Birch-Murnaghan equation of state [4]. Mechanical properties such as bulk modulus, shear modulus, and Young's modulus were computed from the optimized structure. Electronic properties were analyzed by calculating the band structure and density of states (DOS) using an optimized $7 \times 7 \times 7$ k-point mesh and a 50 Ry energy cutoff. The band structure confirmed a direct band gap, suggesting ZrPtSn's potential for thermoelectric and optoelectronic applications.

Phonon dispersion calculations, performed using density functional perturbation theory (DFPT), confirmed the material's dynamical stability due to the absence of imaginary phonon modes. Self-consistent field calculations iteratively solved the Kohn–Sham equations with valence electron wave functions expanded in a plane-wave basis set at a 50 Ry cutoff energy, balancing computational efficiency and accuracy. The Lagrangian theory of elasticity was used to compute elastic properties within the DFT framework. Given the cubic symmetry of the material, three independent elastic constants were evaluated. Using the Voigt, Reuss, and Hill averaging methods, different elastic characteristics were derived. The Voigt approximation assumes uniform strain, while the Reuss approximation assumes uniform stress. Elastic moduli and mechanical properties were assessed as outlined in reference [5].

Results and discussion

Structure of ZrPtSn

A cell relaxation calculation was used to achieve structural optimization, as well as K-points and cutoff energy. Using the relationship of energy volume to the Murnaghan equation of state [4], the volume that produces the minimum energy value was obtained as reported in Table 2. ZrPtSn is half-Heusler structured and crystallizes in the cubic F43m space group. Zr is bonded to four equivalent

Table 1 Calculated bond lengths (Å) for ZrPtSn using GGA-PBE, LDA, and PBEsol

Bond	GGA-PBE	LDA	GGA-PBEsol	References
Zr-Pt	2.76	2.68	2.72	This work
Zr-Sn	3.19	3.11	3.15	This work
Pt–Sn	2.76	2.68	2.72	This work

Table 2 Physical properties of ZrPtSn with and without SOC effects calculated using PBEsol in comparison to DFT studies on similar Zr-based HH compounds

Compound	a_0 (Å)	B (GPa)	B′	V (Å^3)	References
ZrPtSn	6.467	103.2	4.38	67.62	This work (with SOC)
ZrPtSn	6.476	105.1	4.27	67.90	This work (without SOC)
ZrCoAs	5.839	150.7	4.89	49.77	[6]
ZrCoSb	6.099	134.1	4.26	56.72	[7]
ZrCoBi	6.224	119.9	4.14	60.28	[7]

Pt and six equivalent Sn atoms to form a mixture of distorted faces and corner-sharing $ZrSn_6Pt_4$ tetrahedra. The calculated bond lengths are listed in Tables 1, 2.

The calculated bond lengths of ZrPtSn shows slightly overestimated values due to the inherent tendency of the functional to predict longer interatomic distances [4]. When LDA is applied, bond lengths are reduced by approximately 2–3% due to its over binding nature. That is, the Zr-Pt and Pt–Sn bonds uniformly shorten from 2.76 (GGA-PBE) to approximately 2.68 Å (LDA), while the Zr-Sn bond decreases from 3.19 to 3.11 Å. PBEsol, reducing bond lengths by 1–2%. The Zr-Sn bond, being the longest reflects a weaker bonding compared to the Zr-Pt and Pt–Sn bonds. These variations in bond length influence the lattice parameters, elastic properties, and phonon dynamics of ZrPtSn. The shorter bond lengths predicted by LDA and PBEsol may lead to slightly higher bulk moduli and lower ductility compared to those predicted by GGA-PBE. Therefore, while GGA-PBE provides a baseline for general trends, PBEsol emerges as a better choice for more accuracy. Including spin–orbit coupling (SOC) in the calculations is essential for materials like ZrPtSn because of the heavy Pt and Sn. SOC slightly influenced the lattice parameter. The results show a slight reduction in the lattice parameter when SOC was considered, which had an impact on the electronic properties. Further discussion on the effects of SOC on electronic properties of ZrPtSn is provided in "Band structure and projected density of states" section.

Elastic constants and mechanical properties

The calculated elastic constants for ZrPtSn ($C_{11}=181.0$ GPa, $C_{12}=28.0$ GPa, $C_{44}=70.1$ GPa) satisfy the Born stability criteria, confirming mechanical stability. The high C_{11} indicates strong resistance to uniaxial compression, while the relatively low C_{12} suggests some elastic anisotropy. The moderate C_{44} reflects the alloy's shear resistance. Poisson's ratio of 0.30 indicates balanced ductility and brittleness. The universal anisotropy factor ($A_U=0.09$) shows the material is nearly isotropic, confirming mechanical stability and isotropic behaviour under ambient conditions. These values suggest moderate stiffness, ideal for applications requiring structural integrity and mechanical reliability.

The stiffness matrix eigenvalues were computed using the ELATE software [8], which allows for a detailed visualization and interpretation of elastic anisotropy in crystalline materials. For ZrPtSn, the calculated eigenvalues are: $\lambda_1=\lambda_2=\lambda_3=70$ GPa, $\lambda_4=\lambda_5=108$ GPa, and $\lambda_6=402$ GPa. These eigenvalues correspond to the principal modes of deformation in the elastic tensor. The near-degeneracy of λ_1 through λ_3 and λ_4, λ_5 suggests relatively isotropic elastic behavior in certain crystallographic directions, particularly under shear and simple compressive loads. However, the significantly higher value of λ_6 indicates a stronger resistance to deformation in a particular mode, likely associated with directional bonding interactions and the cubic symmetry of the half-Heusler structure. This reflects an underlying elastic anisotropy, which, although moderate, is relevant when considering the material's mechanical reliability under multiaxial stress conditions. The elastic properties were as well analysed using ELATE software, producing consistent bulk moduli ($K=134$ GPa in Voigt, Reuss, and VRH schemes),which indicates isotropic behaviour under compression. Young's modulus (E) ranges from 142.82 to 178.86 GPa, showing minor anisotropy. The shear modulus (G) varies from 54 to 70 GPa, with an average of 63.091 GPa, indicating moderate resistance to shape deformation. Poisson's ratio (ν) ranges from 0.20173 to 0.37976, with an average value of 0.30. This directional variation suggests ductile-like behaviour in certain regions. The eigenvalues of the stiffness matrix show a directional variation in stiffness, with λ_6 reaching 402 GPa, which is supported by the anisotropy indices for Young's modulus (1.252) and shear modulus (1.296). These analyses confirm that ZrPtSn exhibits isotropic properties with subtle anisotropy. ELATE analysis further affirms its moderate stiffness, low anisotropy, and balanced mechanical properties, making it a promising candidate for applications requiring mechanical stability in multiple directions.

Band structure and projected density of states

The electronic structures of ZrPtSn were calculated and reported in Fig. 1a and b. From the electronic band structure calculations, the valence band maxima (VBM) are located at W, whereas the conduction band minima (CBm) are located at L without SOC effects. With the incorporation of the SOC, the positions of VBM and CBM change to near Γ –L, respectively. The compound maintains its properties in indirect bandgap semiconductors with a high reflectivity in the infrared part of the photon energy spectrum as per the magnitude of the bandgaps, which is slightly above 1 eV. For indirect bandgap semiconductors, the conductivity is enhanced by phonon vibrations; which will be discussed later in "Lattice dynamics: phonon dispersion" section. The projected densities of the states in Fig. 1b demonstrate that Zr 3d dominates both the valence band and the conduction bands of the alloy, both with and without SOC effects.

The inclusion of spin orbit coupling (SOC) leads to a noticeable reduction in the calculated bandgap of ZrPtSn from 1.10 eV (without SOC) to 0.95 eV (with SOC). This bandgap narrowing arises primarily due to the strong relativistic effects introduced by the presence of heavy elements, particularly platinum (Pt) and tin (Sn). SOC modifies the electronic band structure by lifting the degeneracy of electronic states near the valence band maximum (VBM) and conduction band minimum (CBM), especially in systems where d- and p-orbitals are dominant. In the case of ZrPtSn, the Zr 3d and Pt 2d orbitals significantly contribute near the Fermi level, and the SOC interaction splits these bands, effectively reducing the energy difference between the VBM and CBM. This behavior is consistent with previous observations in similar HH systems containing heavy atoms,

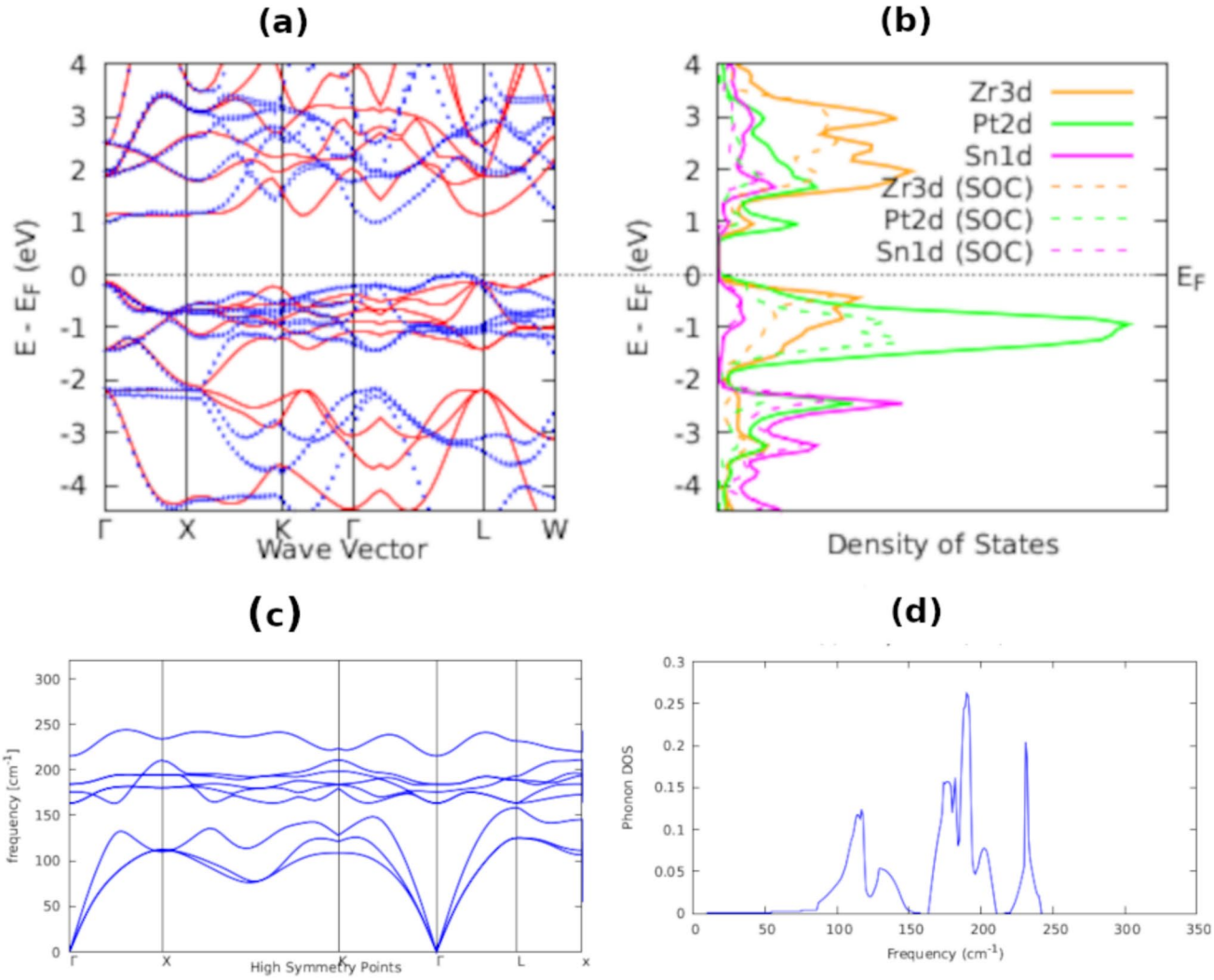

Fig. 1 **a** Calculated Band structures with SOC (dotted blue) and without SOC (red solid lines), **b** Projected Density of States with and without SOC, **c** Phonon dispersion Curves and **d** Phonon Density of states for ZrPtSn

where SOC tends to reduce the bandgap and influence thermoelectric and optical properties [9, 10]. Thus, accounting for SOC is crucial for accurate prediction of electronic properties in such systems.

Lattice dynamics: phonon dispersion

Phonon frequencies are created when the atoms in a crystal are displaced from their rest positions, causing the pressures to increase. Although crystals are expected to be fixed, an increase in temperature can cause the atoms to vibrate about their mean position. The study of the lattice vibration also explains how solids absorb energy. The calculated phonon dispersion curves and density of states for ZrPtSn are shown in Fig. 1c and d. The computations were carried out using the procedure in reference [11], and in the first Brillouin zone representing the primitive cell in the reciprocal lattice. The zone sampled in this work covered Γ–X–K–Γ–L–W–X. Phonons should have nonnegative and real frequencies for stability [12]. Negative frequencies indicate that the potential energy of the system is decreasing, and so the system is unstable. ZrPtSn is dynamically stable since there are no negative frequencies or dispersions as observed in Fig. 1c and d.

Thermal properties

The thermal properties of ZrPtSn were calculated within the temperature range of 0 to 800 K, ensuring the applicability of the quasi-harmonic Debye model. Figure 2a shows that the Debye vibrational energy increases non-linearly with temperature, especially beyond 200 K. This is due to the thermal excitation of phonons. In contrast, the Debye vibrational free energy decreases steadily with temperature, as shown in Fig. 2c. This is driven by the increasing entropic contribution. Figure 2b illustrates that the entropy of ZrPtSn approaches zero at 0 K. This is consistent with the third law of thermodynamics; the material remains ordered in its ground state. With increasing temperature, the system becomes increasingly disordered, explaining the rise of the entropy as a result of enhanced phonon activity. The heat capacity (C_V) of ZrPtSn is calculated using the relation in Eq. 1.

$$C_V = (C_V)_{\text{ele}} + (C_V)_{\text{pho}}, \tag{1}$$

where $(C_V)_{\text{ele}}$ represents the electronic contribution and $(C_V)_{\text{pho}}$ denotes phonon or lattice contributions. The electronic contribution has a linear temperature dependence, while the phonon contribution follows a cubic dependence.

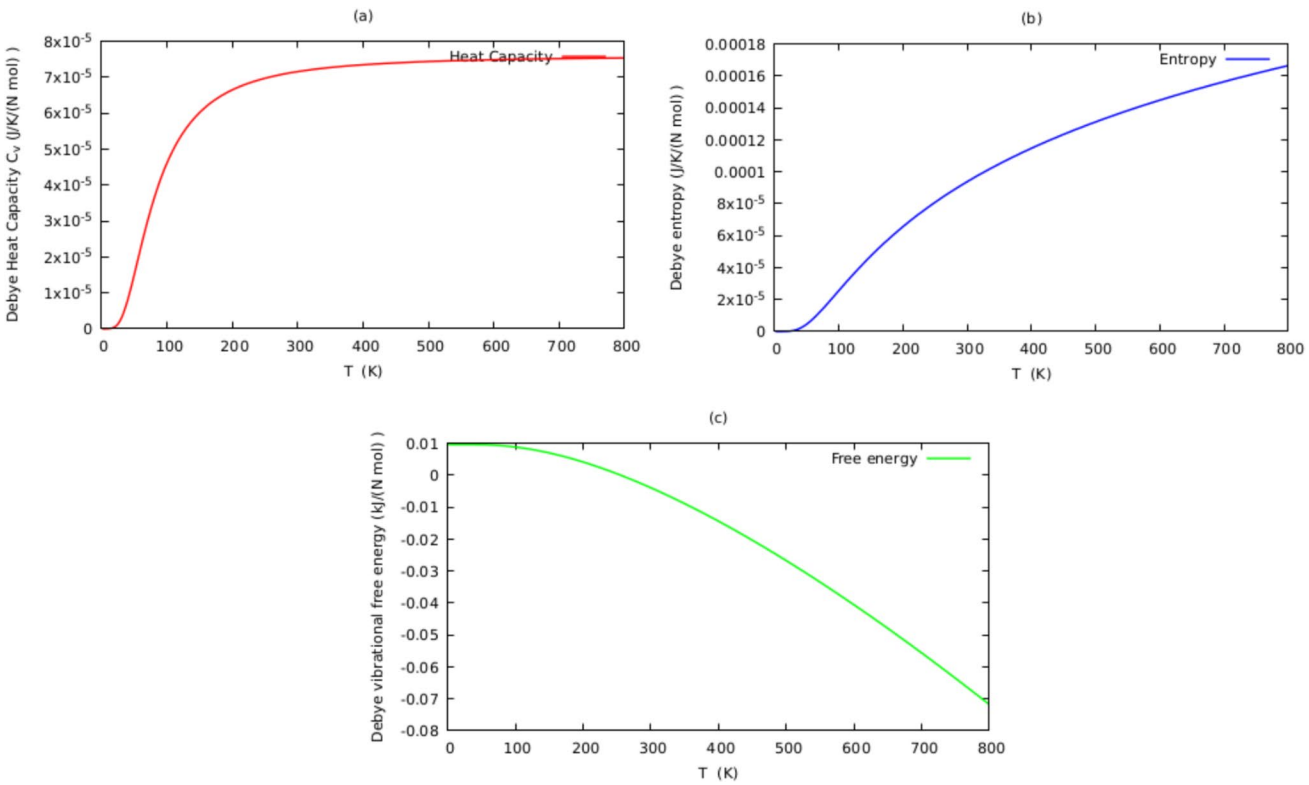

Fig. 2 Thermal properties of ZrPtSn **a** Debyes heat capacity (CV), **b** Debye entropy, and **c** Debye vibrational free energy as functions of temperature

From Fig. 2a, the computed Debye heat capacity (C_V) as a function of temperature demonstrates that $C_V \to 0$ as $T \to 0$, consistent with the Debye model. At low temperatures, the heat capacity of ZrPtSn exhibits cubic dependence ($C_V \propto T^3$), indicating phonon dominance in the material. As the temperature increases, C_V increases due to phonon thermal vibrations, reaching a plateau at high temperatures (beyond 500 K). This plateau corresponds to the Dulong–Petit classical limit, where anharmonic effects are suppressed, and the heat capacity becomes constant. At intermediate temperatures (100–500 K), atomic lattice vibrations dominate the heat capacity behavior. These thermal properties highlight the stability and thermal response of ZrPtSn, which are critical for its potential applications in temperature-dependent environments.

To further evaluate the thermoelectric performance of ZrPtSn, we computed the Seebeck coefficient (S), electrical conductivity (σ/τ), electronic contribution to thermal conductivity (κ_e/τ), power factor and figure of merit (ZT) using the semi-classical Boltzmann transport theory within the constant relaxation time approximation [13] across the temperature range of 300–800 K as shown in Fig. 3. The thermal conductivity showed an increasing trend with temperature, reaching its maximum value of 1.5×10^{16} W/mK at 800 K, suggesting enhanced phonon activity at higher temperatures. In contrast, the electrical conductivity showed a decreasing trend with temperature, with the highest value of 8.5×10^{20} S/m at 300 K, indicating metallic-like carrier mobility that diminishes with thermal scattering. The power factor increased with temperature, with a peak of 1.3×10^{12} W/mK^2 at 800 K, consistent with the enhanced thermoelectric efficiency at elevated temperatures. The Seebeck coefficient demonstrated interesting energy asymmetry, showing higher values at negative energies at 300 K and increasing positively at higher energies near 800 K, highlighting a strong temperature dependence in carrier-type sensitivity and potential for tuning via doping. Finally, the figure of merit (ZT) showed a moderate increase with temperature, reaching 0.14 at 800 K, 0.13 at 600 K, and 0.07 at 300 K, confirming that ZrPtSn has potential for thermoelectric applications, especially in the mid- to high-temperature regime where its transport properties are more favorable. These results are in good agreement with the earlier study of thermoelectric properties of Zr-based HH alloys [11].

To gain a comprehensive understanding of the thermoelectric potential of ZrPtSn, it is useful to compare its performance with full-Heusler (FH) alloys composed of similar elements, such as Zr_2NiSn [11] and $TiNi_2M$, $ZrNi_2M$, $HfNi_2M$ (M = Sn, Ge, Si) [14] compounds. Unlike many FH alloys, which are typically metallic or semi-metallic, ZrPtSn demonstrates semiconducting behavior with a suitable indirect band gap, moderate electrical conductivity, and a relatively low thermal conductivity. These features, coupled with its mechanical robustness and low anisotropy, enhance its suitability for thermoelectric applications. ZrPtSn offers a better balance between thermal conductivity, Seebeck coefficient, and mechanical stability compared to its full-Heusler counterparts, making it a more promising candidate for thermoelectric devices operating in the mid to high-temperature range, where efficient heat to electricity conversion is essential.

Conclusion

In this study, we performed a comprehensive first-principles investigation of the structural, mechanical, electronic, and thermal properties of the ZrPtSn half-Heusler alloy. The compound crystallizes in the stable cubic F-43 m structure, with PBEsol providing a reliable description of its equilibrium lattice parameters. Phonon dispersion curves showed no imaginary frequencies, confirming the alloy's dynamical stability, while elastic constants satisfied the Born-Huang mechanical stability criteria. The calculated moduli and low elastic anisotropy suggest that ZrPtSn possesses good mechanical strength and isotropy, which are favourable for high-temperature device integration. Electronic structure analysis shows that ZrPtSn is an indirect band gap semiconductor, with a band gap of 1.10 eV that reduces to 0.95 eV when spin–orbit coupling (SOC) is included. This reduction is attributed to relativistic effects introduced by the heavy Pt and Sn atoms, which cause band splitting near the Fermi level. The projected density of states indicates that Zr 3d orbitals dominate the valence band, while Pt 3d states shape the conduction band, a configuration that plays a vital role in carrier mobility and transport efficiency. To assess its thermoelectric potential, we carried out temperature-dependent transport property calculations, including the Seebeck coefficient, electrical conductivity, and power factor. The results show that ZrPtSn exhibits a high Seebeck coefficient and favourable power factor value, particularly at elevated temperatures, highlighting its promise for thermoelectric applications. The moderate band gap, combined with SOC-influenced band convergence and stable transport behaviour, indicates that ZrPtSn operates efficiently in mid to high-temperature thermoelectric modules. ZrPtSn demonstrates an excellent combination of mechanical robustness, electronic tunability, and thermoelectric efficiency, positioning it as a promising multifunctional material. These theoretical findings offer a basis for experimental synthesis and application-driven optimization, particularly in the areas of energy conversion and spin-based electronic devices.

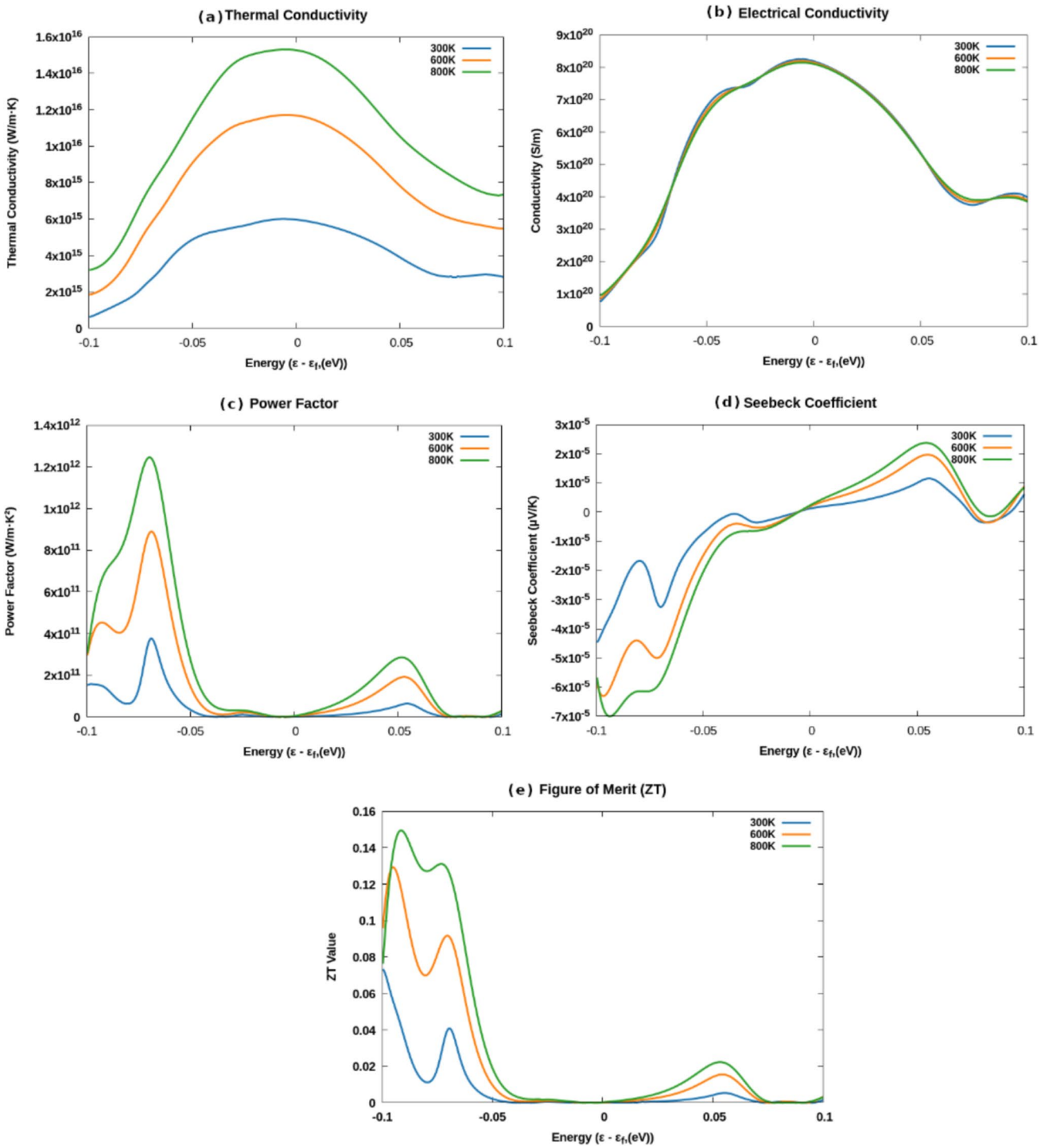

Fig. 3 Thermoelectric properties of ZrPtSn **a** Thermal conductivity, **b** Electrical conductivity, **c** Power factor, **d** Seebeck coefficient and **e** Figure of Merit (ZT), over a temperature range of 300–800 K

This research was supported by PASET through the RSIF program, the ASESMANET EU 2024 research grant from ICTP, and the DOCTAS Research Fellowship Award funded by the Carnegie Corporation of New York. We thank the Scale-Bridging Simulation of Functional Composites ICAMS at Ruhr-Universität Bochum for valuable discussions.

Supplementary Information The online version contains supplementary material available at https://doi.org/10.1557/s43580-025-01314-8.

Author contributions All authors contributed to the research design, analysis, and manuscript preparation. Specific roles and contributions can be provided upon request.

Funding Open access funding provided by University of Pretoria. This work was funded by the PASET RSIF, ASESMANET EU 2024 research grant, DOCTAS Research Fellowship Award and Carnegie Corporation of New York. Computational resources were provided by the CHPC through the project MATS1181.

Data availability All data generated or analyzed during this study are available upon request of the corresponding author.

Materials availability Not applicable.

Code availability Not applicable.

Declarations

Competing interests The authors declare no conflict of interest.

Ethical approval Not applicable.

Informed consent Not applicable.

Consent for publication Not applicable.

Open Access This article is licensed under a Creative Commons Attribution 4.0 International License, which permits use, sharing, adaptation, distribution and reproduction in any medium or format, as long as you give appropriate credit to the original author(s) and the source, provide a link to the Creative Commons licence, and indicate if changes were made. The images or other third party material in this article are included in the article's Creative Commons licence, unless indicated otherwise in a credit line to the material. If material is not included in the article's Creative Commons licence and your intended use is not permitted by statutory regulation or exceeds the permitted use, you will need to obtain permission directly from the copyright holder. To view a copy of this licence, visit http://creativecommons.org/licenses/by/4.0/.

References

1. T. Sekimoto, K. Kurosaki, H. Muta, S. Yamanaka, Thermoelectric properties of Sn-doped TiCoSb half-Heuslercompounds. J. Alloys Compd. **407**(1–2), 326–329 (2006)
2. P. Giannozzi et al., QUANTUM ESPRESSO: a modular and open-source software project for quantum simulations ofmaterials. J. Phys. Condens. Matter. **21**(39), 395502 (2009)
3. J.P. Perdew, K. Burke, M. Ernzerhof, Generalized gradient approximation made simple. Phys. Rev. Lett. **77**(18), 3865–3868 (1996). https://doi.org/10.1103/PhysRevLett.77.3865
4. F. Murnaghan, The compressibility of media under extreme pressures. Proc. Natl. Acad. Sci. U.S.A. **30**(9), 244 (1944). https://doi.org/10.1073/pnas.30.9.244
5. D. Chung, W. Buessem, The Voigt-Reuss-Hill approximation and elastic moduli of polycrystalline MgO, CaF2, β-ZnS,ZnSe, and CdTe. J. Appl. Phys. **38**(6), 2535–2540 (1967)
6. L. Allan, R.E. Mapasha, W.M. Mulwa, J.M. Mwabora, R.J. Musembi, First-principles calculations to investigate theelastic, electronic, dynamical, and optical properties of cubic ZrCoAs half-Heusler semiconductor for photovoltaic applications.Results Mater. **22**, 100558 (2024). https://doi.org/10.1016/j.rinma.2024.100558
7. L. Allan, W.M. Mulwa, J.M. Mwabora, R.J. Musembi, E. Mapasha, An Ab-Initio study of P-type Zrcoy (Y = Sb and Bi)half-heusler semiconductors. Heliyon (2023). https://doi.org/10.2139/ssrn.4443887
8. R. Gaillac, P. Pullumbi, F.-X. Coudert, ELATE: an open-source online application for analysis and visualization of elastic tensors. J. Phys. Condens. Matter **28**(27), 275201 (2016). https://doi.org/10.1088/0953-8984/28/27/275201
9. P. Mavropoulos, I. Galanakis, V. Popescu, P.H. Dederichs, The influence of spin–orbit coupling on the band gap of Heusler alloys. J. Phys. Condens. Matter **16**(48), S5759 (2004). https://doi.org/10.1088/0953-8984/16/48/043
10. K. Dutta, S. Bandyopadhyay, I. Dasgupta, Effect of spin-orbit coupling in noncentrosymmetric half-Heusler alloys. Phys. Rev. B **108**(24), 245146 (2023). https://doi.org/10.1103/PhysRevB.108.245146
11. L. Allan, R. Musembi, B. Aduda, First principles study of the structural, mechanical, electronic, and lattice dynamical properties of the half-Heusler alloys ZrCoY (Y = Sb, Bi). Mater. Sci. (2022). https://doi.org/10.48550/arXiv.2204.03759
12. A. Togo, First-principles phonon calculations with phonopy and phono3py. J. Phys. Soc. Jpn. **92**(1), 012001 (2023). https://doi.org/10.7566/JPSJ.92.012001
13. G.K. Madsen, D.J. Singh, BoltzTraP. A code for calculating band-structure dependent quantities. Comput. Phys. Commun. **175**(1), 67–71 (2006). https://doi.org/10.1016/j.cpc.2006.03.007
14. E. Tindibale, W.M. Mulwa, B.I. Adetunji, Elastic, anisotropic, lattice dynamics and electronic properties of XNiM and XNi_2M (X = Ti, Zr, Hf; M = Sn, Ge, Si): DFT comparison study. Phys. B **665**, 415029 (2023). https://doi.org/10.1016/j.physb.2023.415029

Publisher's Note Springer Nature remains neutral with regard to jurisdictional claims in published maps and institutional affiliations.